6.2 Salinization Features and Remote Sensing

To detect salt-affected areas and to understand the salinity mechanisms occurring in the study area, remote sensing data and techniques were used in this study with the following aims:

1) to study the geologic features visible on satellite imagery and their related subsurface conditions corresponding to the salinity, and
2) to detect and recognize salt-affected areas both by visual interpretation and digital classification.

To reach these objectives, drainage, lineament and salt-affected areas visible on the satellite images were interpreted. Unsupervised and supervised land use classification, and indices analysis were applied to the satellite image data. The results were compared with the results of visual interpretations.

6.2.1 Results from Visual Interpretation

6.2.1.1 Drainage Pattern in the Study Area

The traces of drainage pattern of the study area are shown in Figure 6.18 and can be simply categorized as follows:

1) **Areas of Structural-controlled Drainage Pattern**
   The drainage pattern in these areas are controlled by geological structures, e.g. anticlinal and synclinal structures, and mostly represented at the north, west and south rims of the study area. The drainage patterns consist of trellis, rectangular and parallel pattern (Figure 6.18a).
2) **Areas of Fine-dendritc to Dendritic Pattern**
   These sorts of drainage patterns mostly appeard in the central plain at the center of the study area where it is almost flat and filled up with fine- to very fine-grained sediment supported by small streams and courses distributed from Mun and Chi River (Figure 6.18b).
3) **Areas of Deranged Pattern**
   Deranged pattern is the disordered pattern. In the study area, this pattern mostly represents in the various sizes of the depression areas, and also in marshy and swampy areas where soluble materials are supposed to lie beneath, especially at the west, south and north rims of the study area where they are the boundaries of the Maha Sarakham Formation and other competent rock units (Figure 6.18c). And it also occurs at the great central plain in the Mun River where the run off water is collected in the ponds, swamps, and marshes.

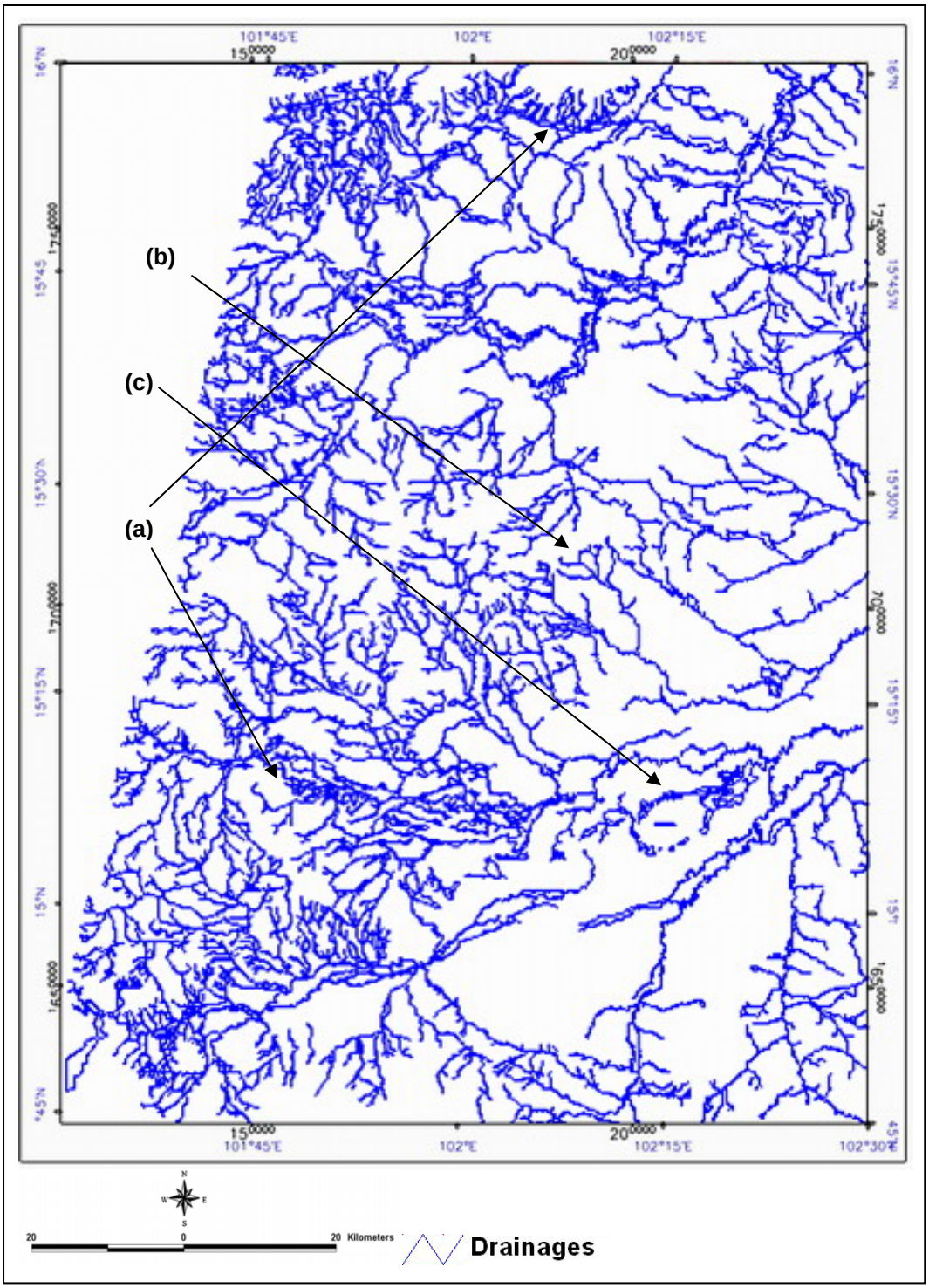

Figure 6.18 Drainage patterns in the study area showing three of drainage pattern types: 1) structural control pattern (a), 2) fine dendritic to dendritic pattern (b), and 3) deranged pattern (c), respectively.

6.2.1.2 Lineament Detection on Satellite Images

The lineaments were grouped into two classes based on the basis of their statistical distribution as follows:

1) Lineaments of First Order represented and repeated on at least 5 images (represent in thick red lines in Figure 6.19)

2) Lineaments of Second Order represented and repeated on at least 3 images (represent in thin red line in Figure 6.19)

More than two hundred lineaments were measured from the lineament map produced from the lineament analysis. The study area as shown in Figure 6.19 was divided into three major parts, the northern, central and southern part. Figure 6.20 shows predominant lineament trends of the upper, the middle, the lower and the entire area. The result can be summarized as follows:

- The predominant lineament trends of the northern part are $N30^{o}$–$40^{o}W$ and also $N30^{o}$-$40^{o}E$;
- The predominant lineament trends of the central part are $N70^{o}$-$80^{o}E$, and another major trend $N10^{o}$-$20^{o}W$;
- The predominant lineament trends of the southern part are $N10^{o}$–$20^{o}W$ and again 60^{o}-$70^{o}W$;
- The predominant lineament trends of the entire area are $N10^{o}$–$20^{o}W$ and $N70^{o}$-$80^{o}E$.

The lineaments on the Tertiary age rocks in the study area are believed to reflect structures of older rock lying below. The predominant lineament trends of the entire area, $N10^{o}$–$20^{o}W$ and $N70^{o}$-$80^{o}E$, correspond to the second deformation (F_2) and, more or less, the third deformation (F_3) based on the study of Chauviroj (1997), respectively. According to Tapponier *et al.* (1986) the Himalayan orogeny is the result of the collision between the Indian plate and China plate in the Lower Tertiary. Consequently, the lineaments in the direction northwest-southeast are affected by the compression in northeast-southwest direction. Later on, the prolongation of the Himalayan orogeny probably induced the updoming and the third deformation in the Miocene-Pleistocene age. The direction of compression movement is interpreted as northwest-southeast. Consequently, the lineaments resulting from the third deformation are normally in northeast-southwest direction.

The lineaments in northwest-southeast and northeast-southwest direction are believed to be the preferred path for the saline groundwater migrating to the surface and causing salinity. This view corresponds to the results from visual interpretation and supervised classification that most of the saline areas occur on the lineaments in northeast-southwest and northwest-southeast direction.

Figure 6.19 Lineament map interpreted from Landsat 7 ETM+ imagery covering study area.

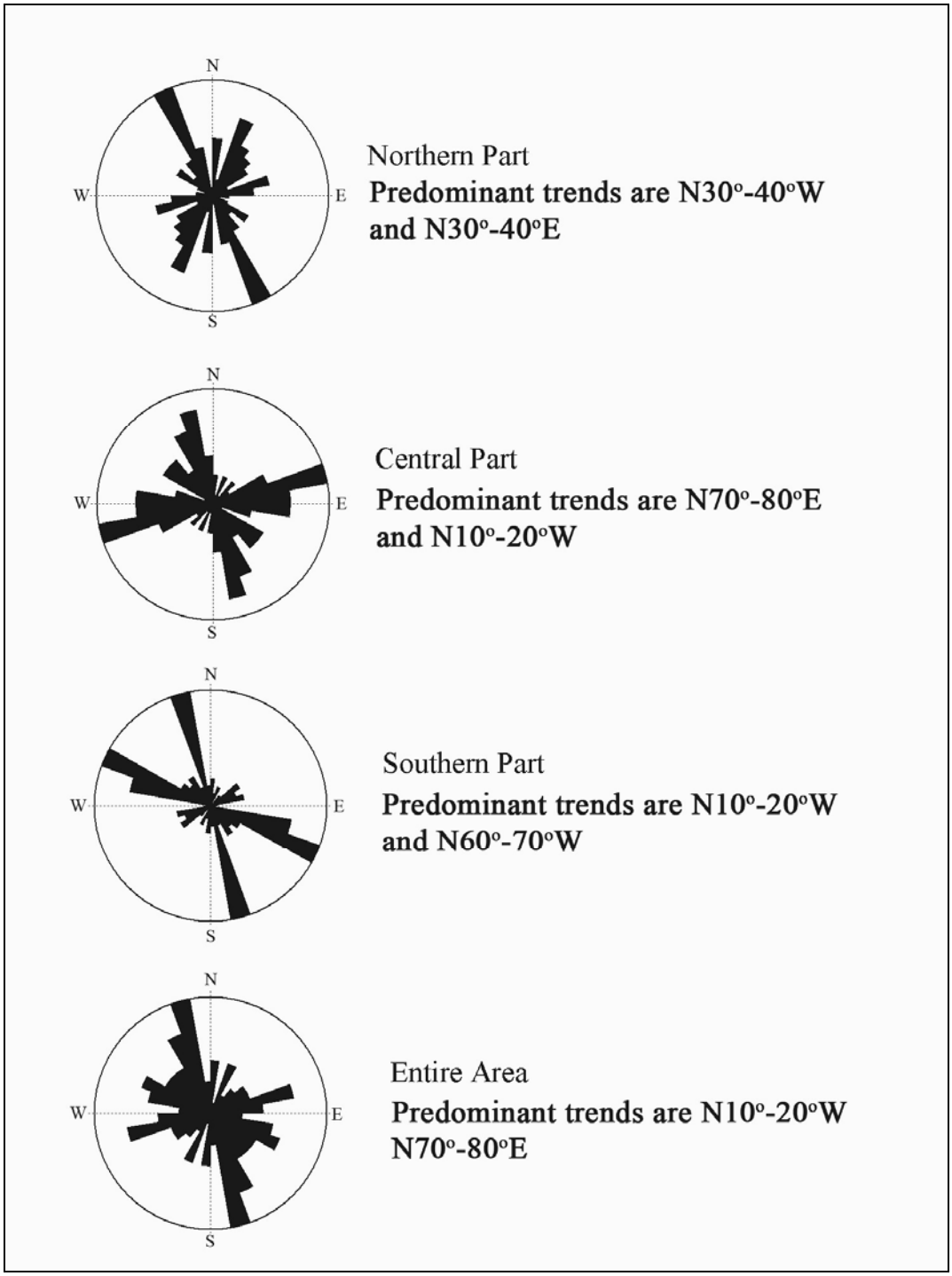

Figure 6.20 Rose diagram showing predominant lineament trends of the northern, the central, the southern part and the entire area of the study area.

6.2.1.3 Distribution of the Salt-affected Areas on Satellite Images

As previously mentioned, the rock salt underlies the study area with variations in range of depth and thickness. This situation plays an important role for the salinity both in terms of level of salinity and its distribution.

a) Salt-affected Areas Characterized by Salinity Levels

Based on visual interpretation of Landsat 7 and ASTER satellite images, coupled with ground truth, this study categorized the salt-affected area into three salinity levels: 1) severe salinity, 2) moderate salinity, and 3) slight salinity, respectively.

1) Severe salinity mostly occurs where the rock salt or salt-bearing rock crops out near to the surface, and also along the boundary of the Maha Sarakham Formation and its underlying Khok Kruat Formation, and where shallow groundwater is present, e.g. in the Dan Khun Thot District (Figure 6.21). On the False Color Composite image of Landsat 7 and also on the False Color Composite image of ASTER, the severely salt-affected areas are mostly presented in very bright or very white color with some small amounts of other colors. The texture of these areas is very fine.

2) Moderate salinity is mostly present along the rivers and tributary plains where the brine comes from shallow interflow and sometimes from deeper groundwater flow. These can play the role of carrying and migrating dissolved salt seepage at the discharge area, e.g. the Mae Nam Mun Valley and its flood prone area in the southern part and Mae Nam Chi Valley and its flood plain area in the northern part of the study area, and also take place along the lineament features within the Basin, e.g. the lineament features at Khong District area (in the blue rectangle shown in Figure 6.21). Moderately salt-affected areas are normally shown in light blue color on the False Color Composite image of Landsat 7 and also on the False Color Composite image of ASTER. They also show fine texture with few mottled spots of other colors.

3) Slightly salt-affected areas are present where salt rock is deeply buried and covered with impervious layers and has no migration path of brine to the surface, e.g. the area among Jaturat, Khong, Bua Yai District (in the green rectangle shown in Figure 6.21), and also other high escarpment areas in the western, southern and northern rims of the Khorat Basin. They are normally shown in pinkish white color on the False Color Composite image of Landsat 7 and also show the same color on the False Color Composite image of ASTER. They normally show a few red or pink mottled textures.

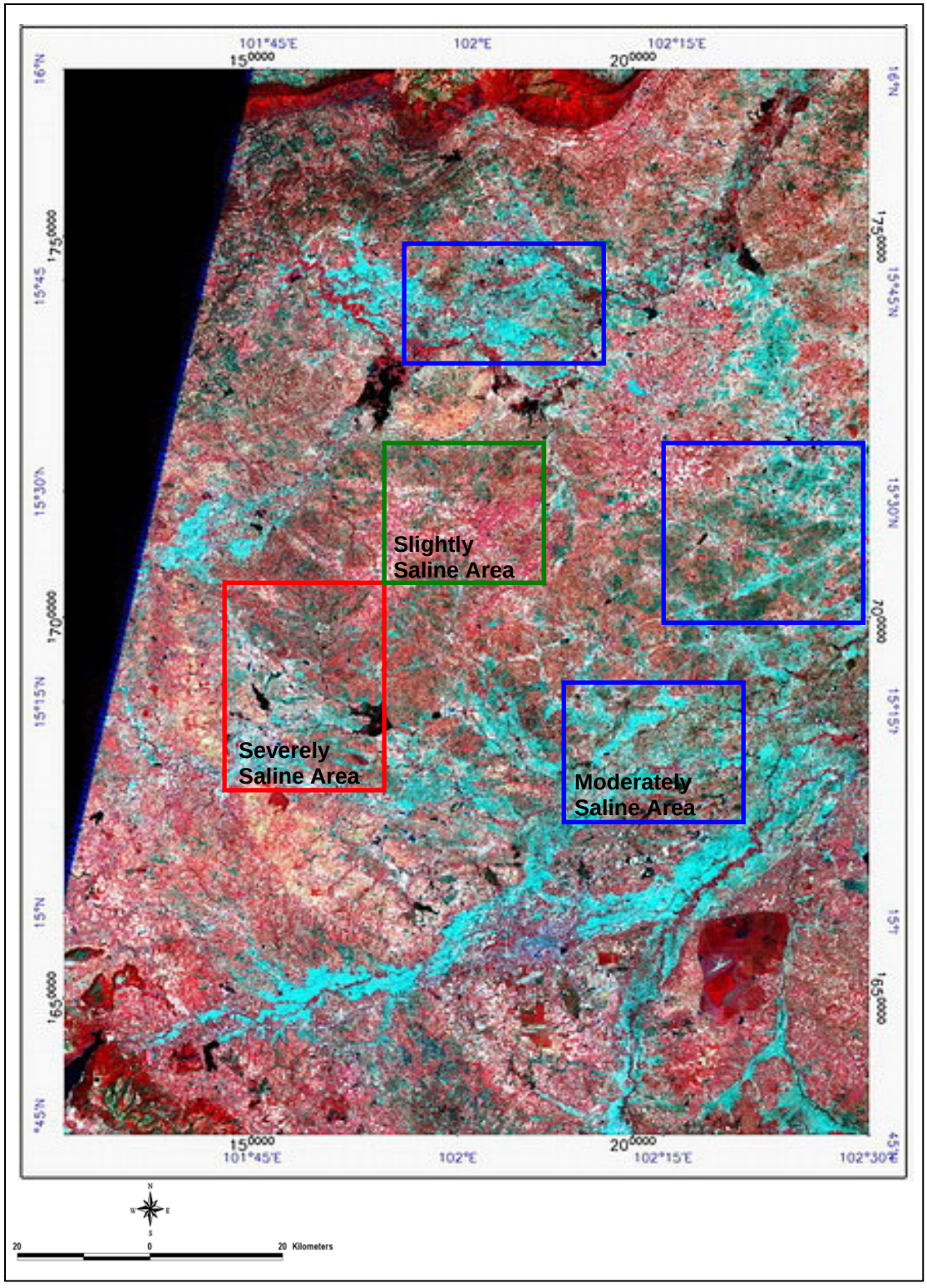

Figure 6.21 False Color Composite image of Landsat 7 acquired on December 27, 1999, bands 4, 3, 2 as red, green, blue shows the severely saline areas in white or bright color (within red rectangle), the moderately saline areas in light blue color (within blue rectangle), and the slightly/non-saline areas in pink/orange/red color (within green rectangle).

b) Salt-affected Areas Characterized by Topographic Conditions

Modified after Wongsomsak (1986) and Takaya *et al*. (1984), the salinity area distribution in the study area could be classified and grouped into 2 categories based on its related topographic and geologic conditions:

1) Hill salt-affected areas,
2) Valley salt-affected areas.

The conceptual diagram showing the relationship between salinity area and geologic setting in the study area is shown in Figure 6.22.

1) Hill Salt-affected Areas

Covered mostly by large and small hills, this area is located to the west of the study area, e.g. in Dan Khun Thot District, Jaturat District, and some part of the central part of the study area, e.g. in Non Thai District area. Geologically, these areas are underlain by the Rock Salt Member of the Maha Sarakham Formation. Salt appears in this area either directly on the Maha Sarakham Formation itself and/or in the foothills due to the seepages.

2) Valley Salt-affected Areas

This sort of salt-affected areas covers most of the valley and its tributaries, e.g. Mae Nam Mun River to the south and Mae Nam Chi River to the north, throughout the study area. The mechanism of salinization in the valley areas is a mixing process and more complex than those of the hill salt-affected area. The salt in the valley area is precipitated from brine that is carried by either surface and/or subsurface water. Brine interflow under cap clay is the major mechanism of salt supply together with some brines from deep groundwater convection along preferred migration paths, e.g. fault and/or fracture planes with the help of capillary rise effect when brines come up to the capillary fringe zone. The valley floor is usually covered by thin recent alluvium overlying sediments of the Plio-Pleistocene Formation.

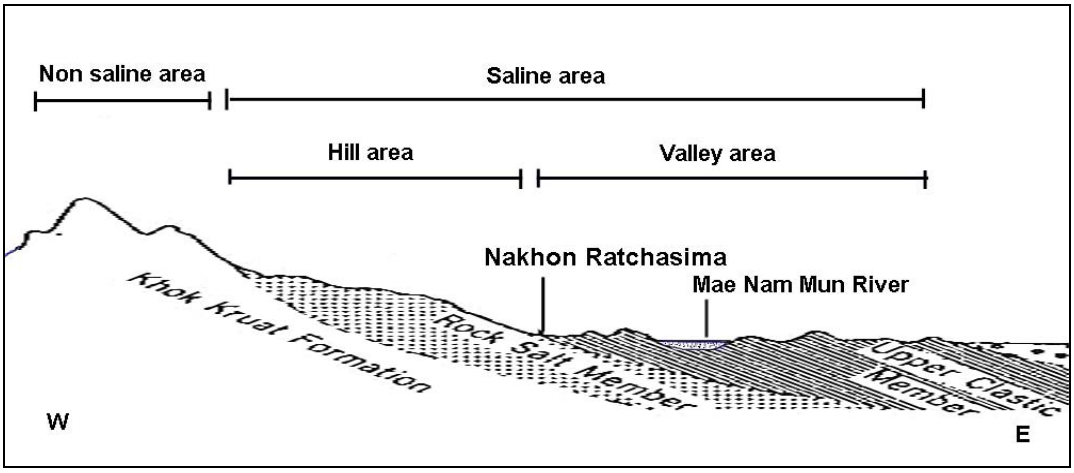

Figure 6.22 A preliminary conceptual diagram the relationship salinity area and the geologic setting (modified after Takaya *et al.*, 1984).

6.2.2 Results from Digital Classification

6.2.2.1 Results from Unsupervised Classification

Apart from visual interpretation on satellite imagery to determine possible salt-affected areas, the satellite images were also classified using ENVI software, both by unsupervised IsoData classification and supervised Maximum Likelihood classification method.

The result from IsoData classification of Landsat 7 and ASTER data are shown in Figure 6.23 and Figure 6.24. The results from IsoData classification show the general idea that land use in the study area can be properly categorized into a maximum of 7 classes or less. Based on background knowledge, i.e. geographic information, geology, the results of this automatically classification can be summarized as follows:

Land use classified from Landsat 7:

- Class 1 represents the water bodies;
- Class 2, 3, and 4 represent forest (both plantation and natural), including water plants;
- Class 5 and 6 represent cash crops or up-land crops;
- Class 7 represents salt-affected areas and/or bare ground.

Land use classified from ASTER

- Class 1 and 2 represent water bodies;
- Class 3 and 4 represent forest, including water plants;
- Class 5 and 6 represent cash crops and/or up-land crops;
- Class 7 represents salt-affected areas and/or bare ground.

In general, results from the unsupervised IsoData of ASTER show more differentiable feature between each class especially saline and non saline area than those of Landsat 7.

6.2.2.2 Results from Supervised Classification

The results from Maximum Likelihood classification of Landsat 7 and ASTER data are shown in Figure 6.25 and Figure 6.26. These results can be summarized as follows:

- The crops and water body classes from both Landsat 7 and ASTER are similar. Especially the water body class gives well distinguishable features from other classes.
- The settlement and the forest class of Landsat 7 are more reliable than those of ASTER due to the fact that it has more samples of these features.
- The salt-affected areas classified from ASTER data are less than those got from Landsat 7 data. Some paddy fields of the western part area are classified as salt-affected areas on ASTER.

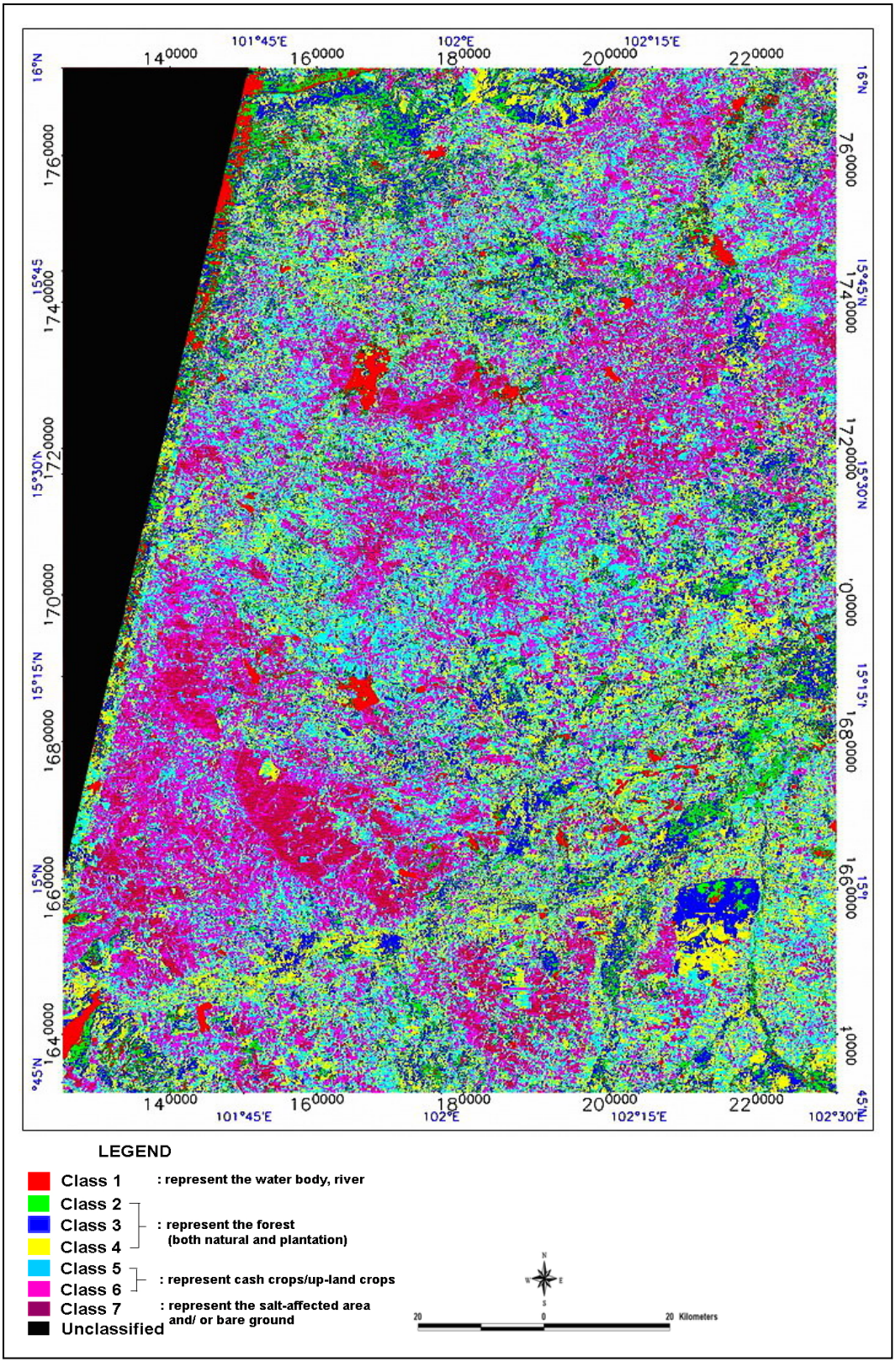

Figure 6.23 Unsupervised IsoData classification image of Landsat 7 acquired on December 27, 1999, with 7 classes.

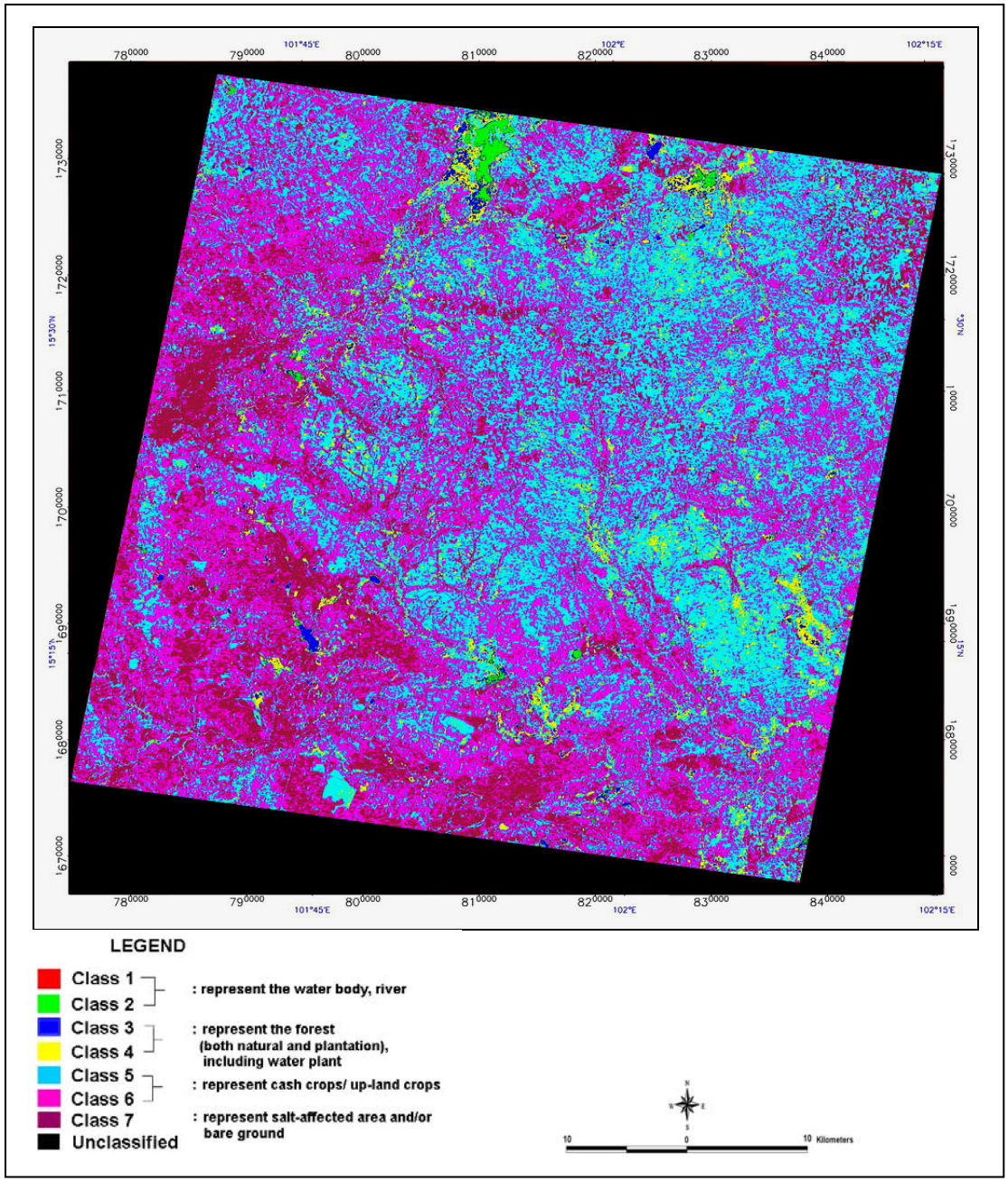

Figure 6.24 Unsupervised IsoData classification image of ASTER acquired on December 7, 2001, with 7 classes.

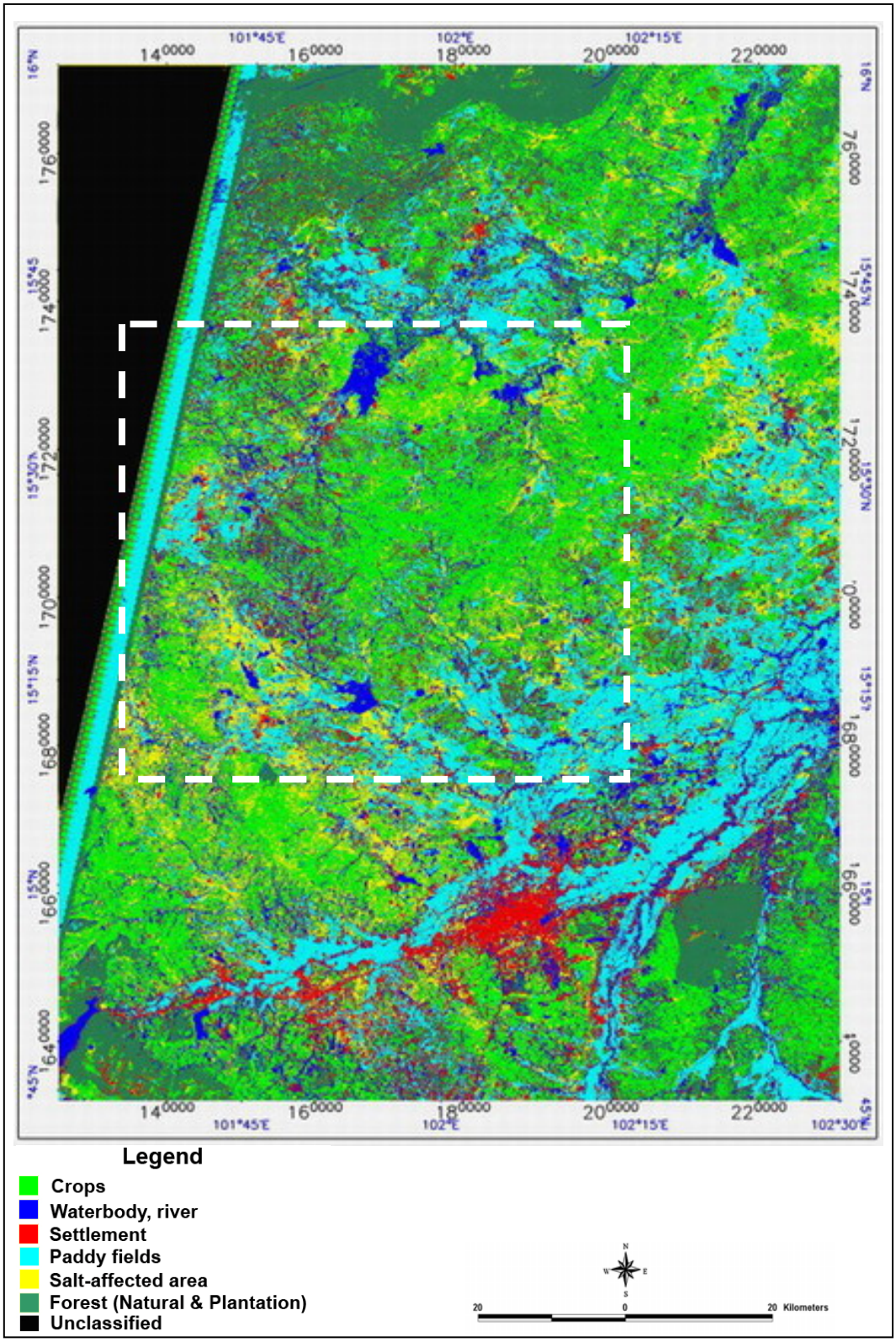

Figure 6.25 Results from the supervised Maximum Likelihood classification of Landsat 7 data. The white rectangle shows the area of the ASTER data scene.

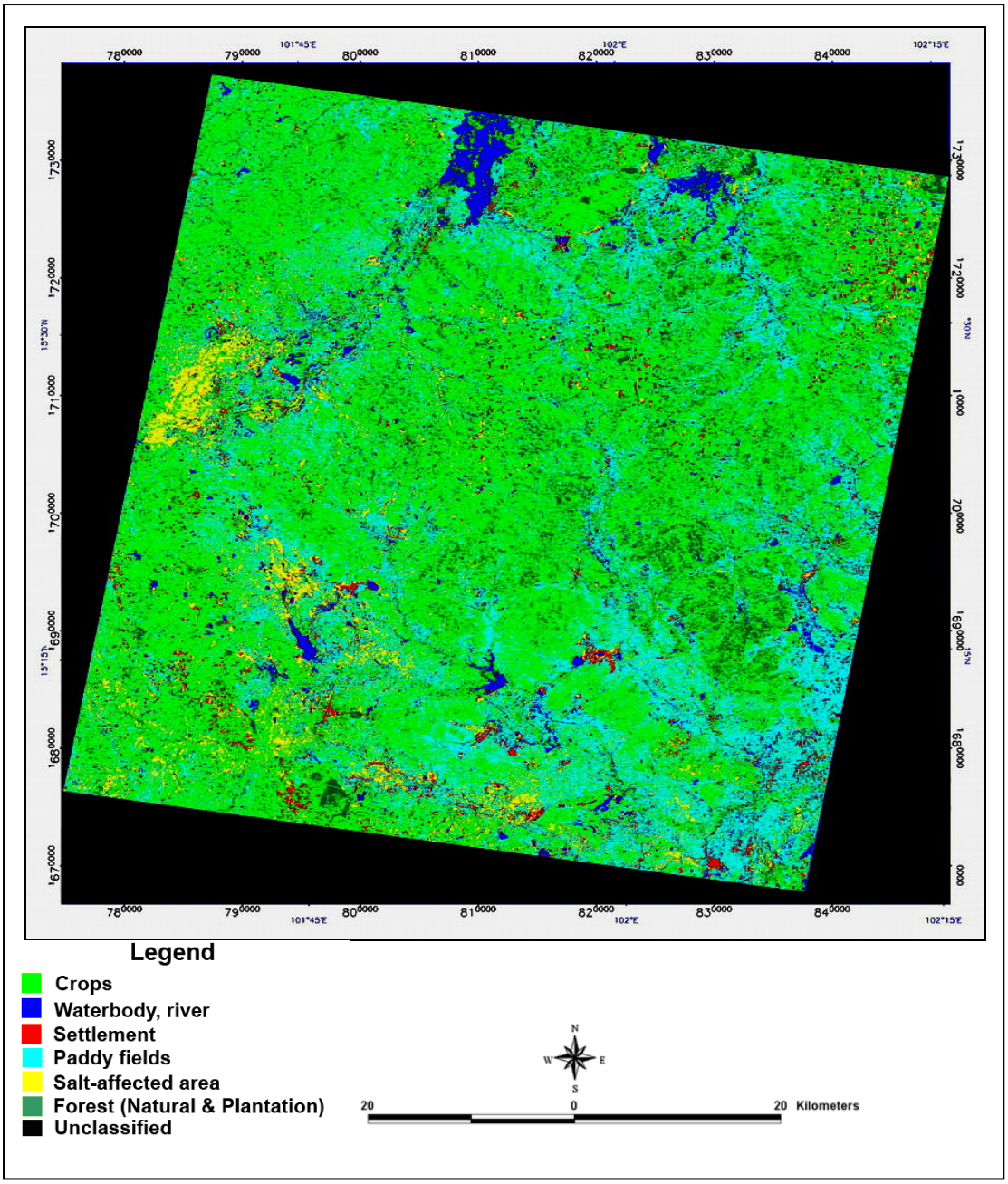

Figure 6.26 Results from supervised Maximum Likelihood classification of ASTER Data acquired on December 7, 2001.

In the field checks conducted between October 15 – December 15, 2003, and January 21 – January 30, 2005, from 128 investigation sites expected to be salt-affected from supervised classification, 120 sites showed salt crust at the surface, and the rest of 8 sites also have potential for salinity since they are covered by salt-like plants. Therefore, the accuracy of this supervised classification to define the salt-affected area is 93.75 percent. Although the accuracy of this classification technique is satisfactory, the selected investigation sites were only located in low land areas while some signs of salt-affected areas, bright or white areas, also shown in elevated areas which is the bare ground in fact, e.g. in the west hills and slopes of the study area. Therefore, the band math technique was employed to eliminate or reduce these problems.

6.2.2.3 Results from Indices Analysis

After getting the potential and/or salt-affected areas from image classification, different remote sensing indicators such as the Salinity Index (SI), the Normalized Differential Salinity Index (NDSI), the Normalized Vegetation Index (NDVI) and the Brightness Index (BI) were employed to study how these indices work for salt-affected areas in the study area.

Results from the indices analysis of the Landsat 7 data showed that the indices that gave acceptable satisfactory results in distinguishing saline area from non-saline area were NDSI and NDVI. The post-processing results of NDSI and NDVI images by density slicing and band thresholding are shown in Figure 6.27 and Figure 6.28. The results from the indices analysis of Landsat 7 data can be summarized as follows:

- After the NDSI image had been enhanced by density slicing and band thresholding, the salt-affected and potential salt-affected areas, depicted in white color, could be roughly differentiated from those of non salt-affected areas, water bodies (in blue color) and vegetation (in green color).

- However, this method could not differentiate salt-affected areas from bare ground consisting of sandy soil to fine sand, located both in low land and elevated areas. This NDSI image also could not discriminate water bodies from the high moisture areas such as dense forests, swamps and marshy areas. Therefore it shows larger areas of water than justified by the real conditions.

- The enhanced NDVI image shows more specific localites of salt-affected or potential salt-affected areas. However, it still shows a mixture water body and areas of high moisture, as in NDSI image.

- The enhanced images of the Salinity Index (SI) and the Brightness Index (BI) of Landsat 7 data are shown in Figure 6.29 and 6.30. However, their results can not distinguish saline from non-saline areas, as the NDSI and NDVI images can.

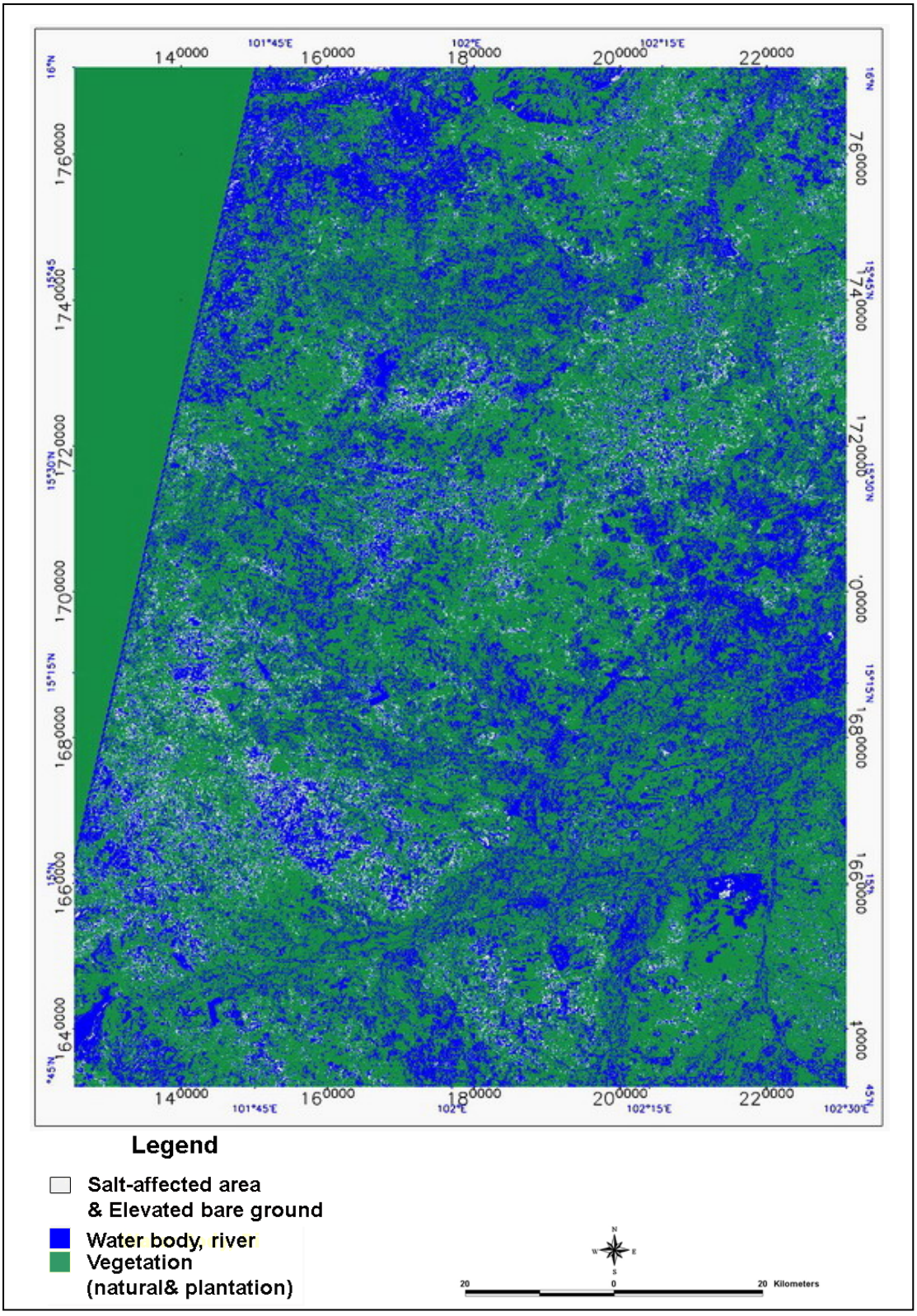

Figure 6.27 Image derived and generated from the Normalized Differential Salinity Index (NDSI) and additional density slicing and band thresholding of Landsat 7 data acquired on December 27, 1999, showing salt- affected or potential salt-affected areas in white color.

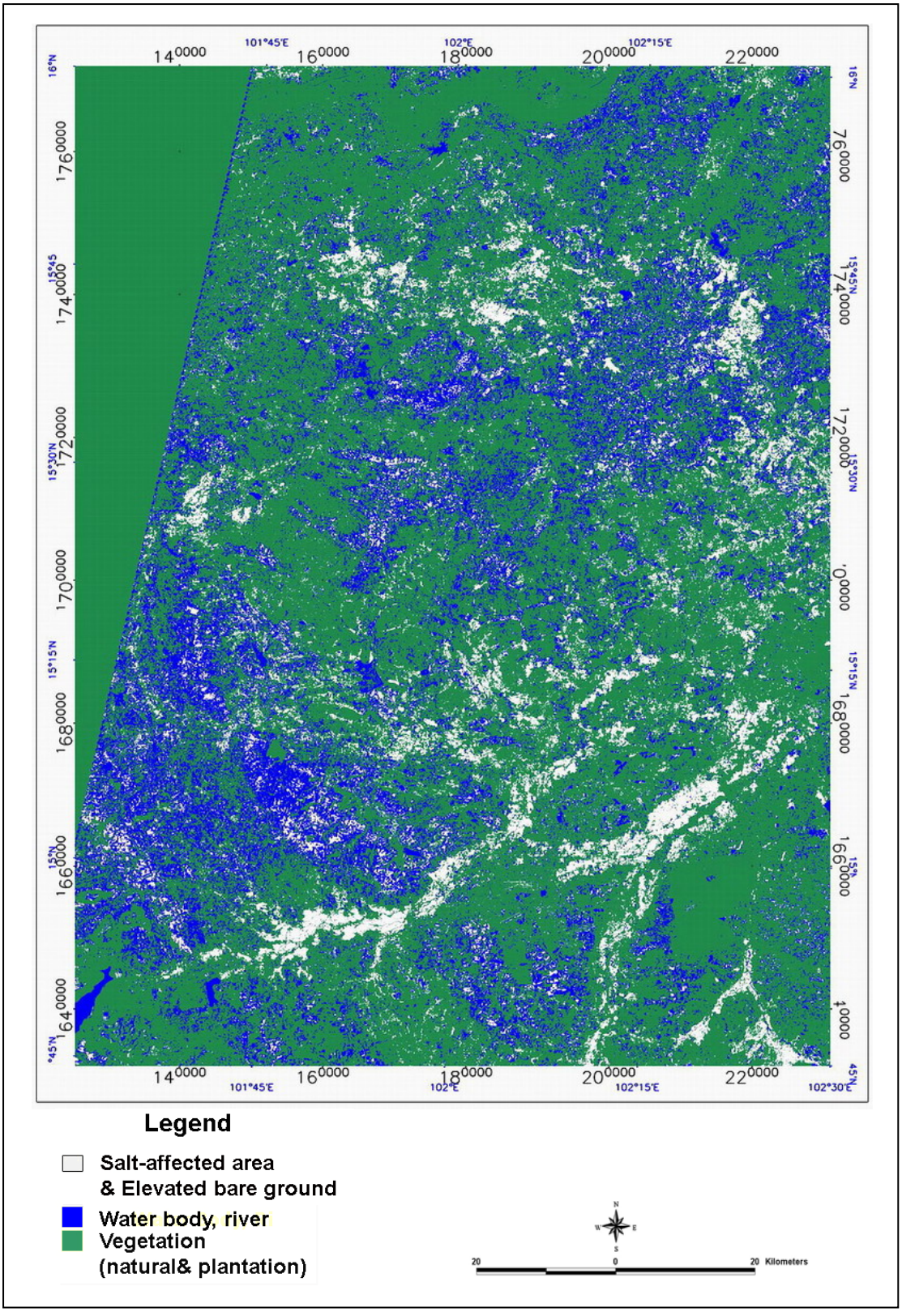

Figure 6.28 Image derived and generated from the Normalized Differential Vegetation Index (NDVI) and additional density slicing and band thresholding of Landsat 7 data acquired on December 27, 1999, showing salt-affected/potential salt-affected area in white color.

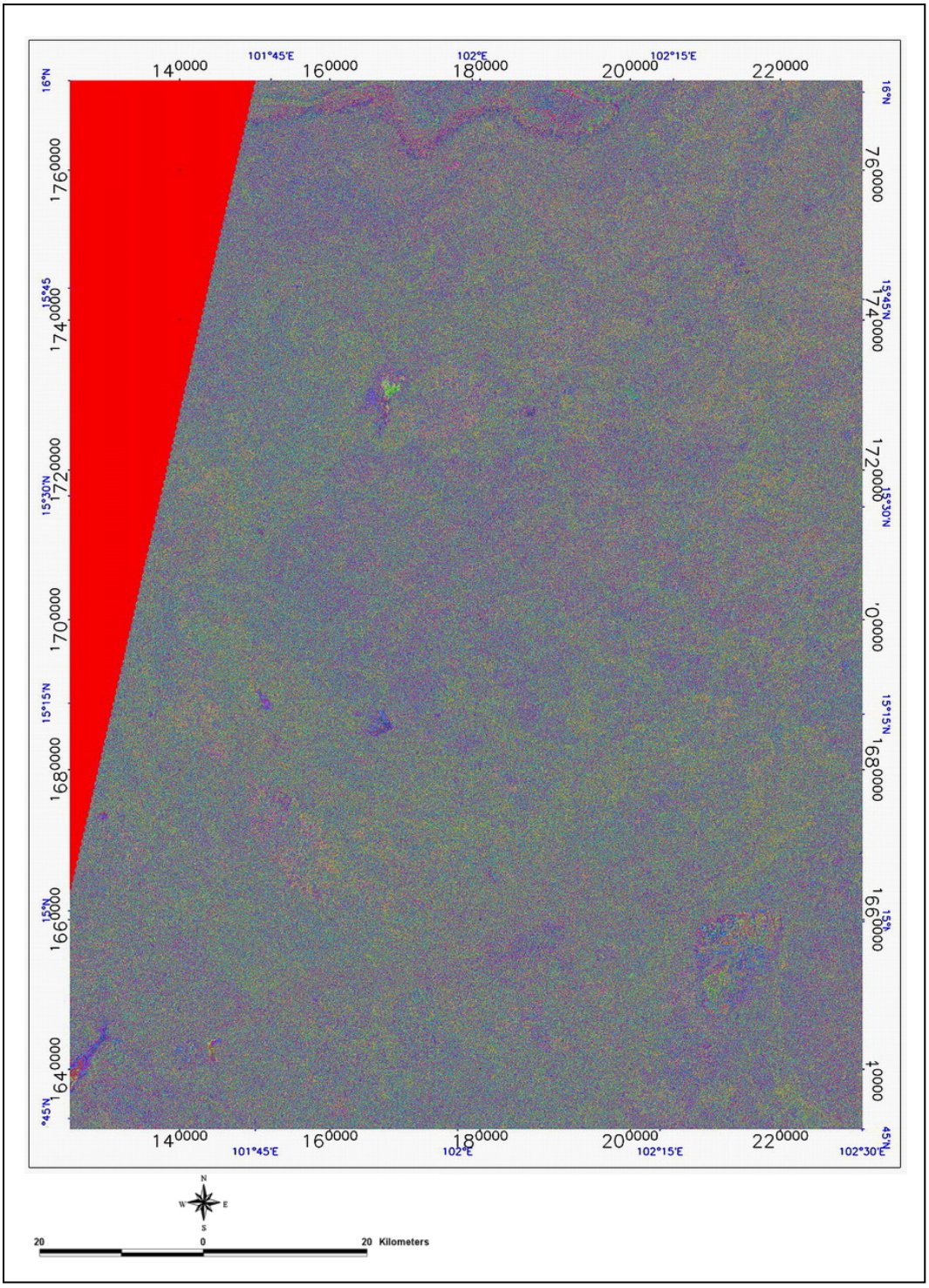

Figure 6.29 Image derived and generated from Salinity Index (SI) and additional density slicing and band thresholding of Landsat 7 data acquired on December 27, 1999.

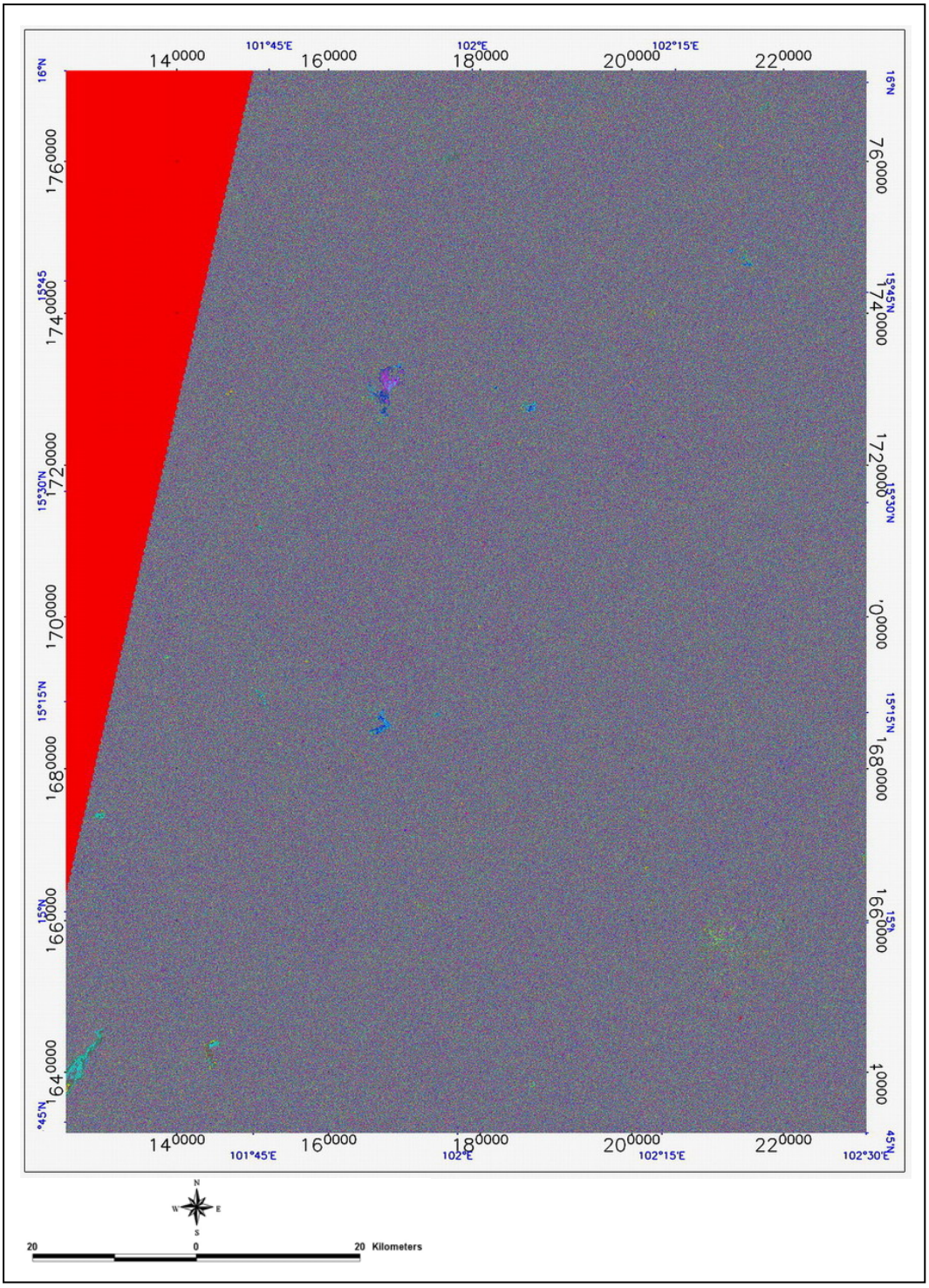

Figure 6.30 Image derived and generated from Brightness Index (BI) and additional density slicing and band thresholding of Landsat 7 data acquired on December 27, 1999.

The NDSI and NDVI images of ASTER data, enhanced by density slicing and band thresholding are shown in Figure 6.31 and Figure 6.32. The results from indices analysis of ASTER data can be summarized as follows:

- The NDSI and NDVI images derived and generated from ASTER data give more satisfactory results in distinguishing saline from non-saline areas than those derived from Landsat 7 data.

- On the NDSI image derived from ASTER data the salt-affected and/or potential salt-affected areas could be more reliably located and differentiated from non salt-affected areas including bare ground on elevated and low land than in Landsat 7 NDSI and NDVI images.

- Moreover, the water bodies could be more precisely differentiated from the high moisture areas than those of Landsat images both on NDSI and NDVI images as well. However, the NDVI image derived from ASTER data also could not differentiate bare ground from salt-affected areas.

After employing indices analysis, the ambiguous salt-affected areas derived from the previous digital image classification technique in high land or elevated areas could be removed and better mapped as compared to previous maps derived from land use classification as shown in NDSI image of ASTER data. Therefore, it is very useful for future work to apply this method to other ASTER scenes in order to detect and locate the salt-affected areas in the Khorat Plateau with higher accuracy.

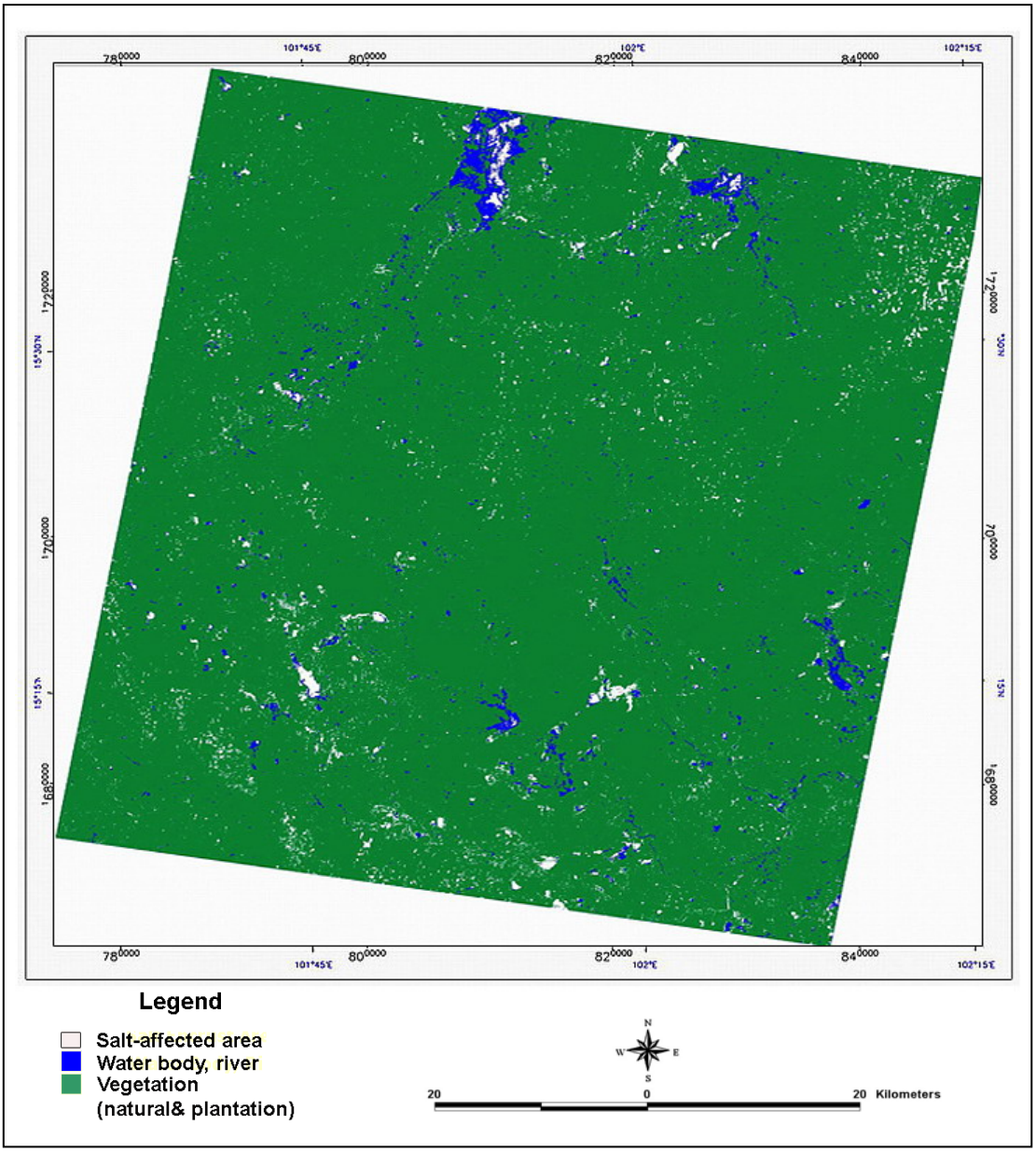

Figure 6.31 Image derived and generated from NDSI and additional density slicing and band thresholding of ASTER data acquired on December 7, 2001, showing salt-affected areas in white color.

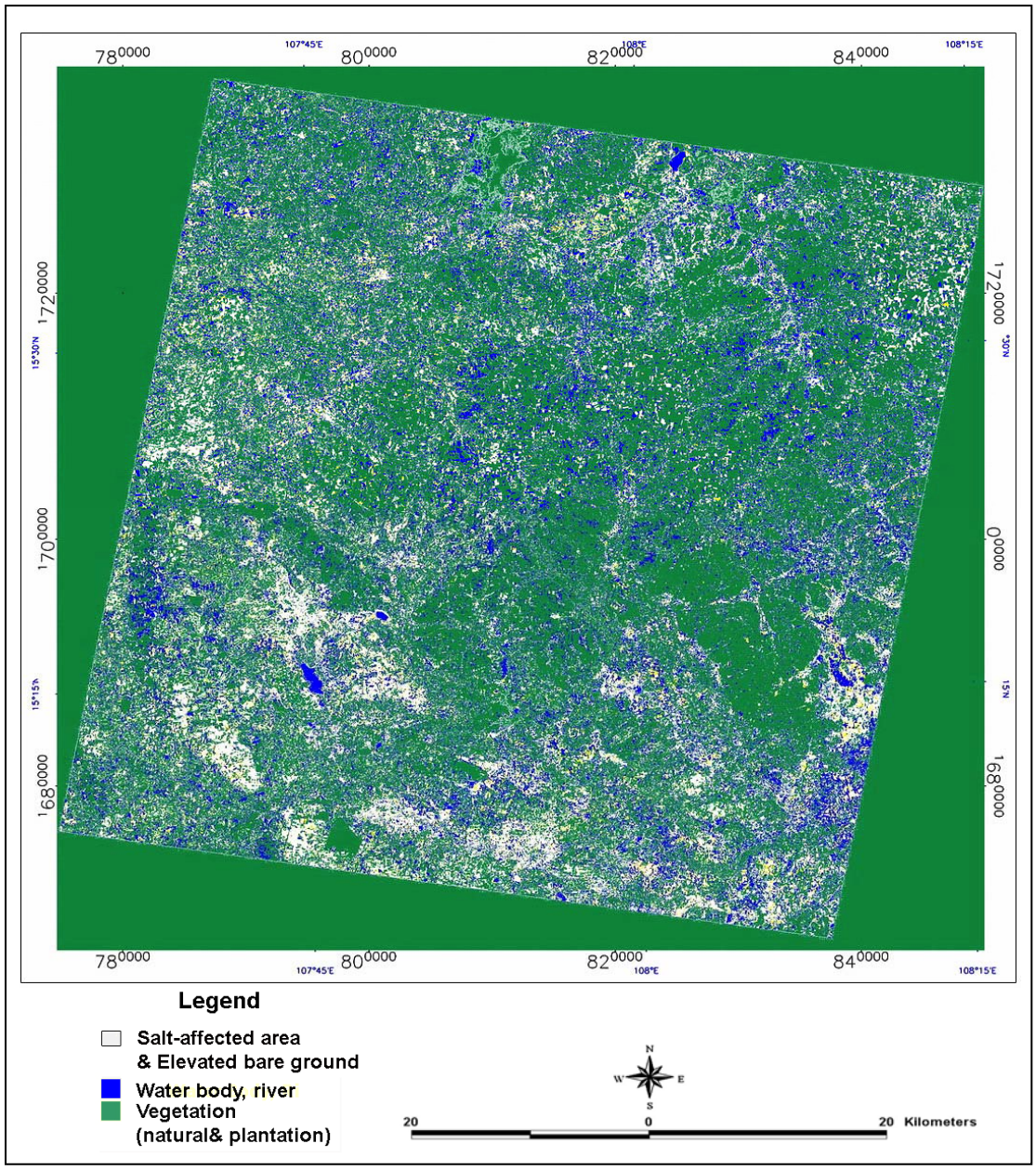

Figure 6.32 Image derived and generated from NDVI and additional density slicing and band thresholding of ASTER data acquired on December 7, 2001, showing salt-affected areas in white color.